Variations in magnetotelluric response functions caused by Sq currents

Shinya Sato*

* Graduate School of Engineering, Kyoto University

Email: sato.shinya.27s@st.kyoto-u.ac.jp

Abstract

The magnetotelluric (MT) responses of the Earth are biased by spatially heterogeneous source fields. Recently, such biases have been reported even in mid-latitude areas, where localized source currents rarely flow. This study focuses on shifts in the MT responses arising from variations in the focus latitude of the solar quiet (Sq) current. The MT responses at 60 s were calculated by changing the center of the Sq current. Slight variations in the focus latitude cause large shifts in the apparent resistivity and phase. During periods of quiet geomagnetic activity, the center varies within a wide range of 20–45° N, whereas this range narrows when there are disruptions. Even though this study considers only a limited case, the results demonstrate the instability of the impedances in periods of quiet geomagnetic activity and a correlation of the MT responses with the magnitude of the geomagnetic activity. As a consequence, even when a station is located at mid-latitudes, the impedances need to be treated carefully for time-lapse MT soundings, for example, by checking the ionospheric current conditions and their dependence on the geomagnetic activity.

Introduction

The magnetotelluric (MT) method is an electromagnetic (EM) exploration technique used to imagine subsurface resistivity structures. Electrical impedances are calculated from the measured EM fields, the origins of which are usually the ionospheric current. The targets of MT surveys are various, for example, buried active faults (Ichihara et al. 2019), volcanic areas (Hata et al. 2020), and deep structures such as the mantle (Evans et al. 2005; Matsuno et al. 2020). Time-lapse MT soundings have also been used to discuss temporal variations in subsurface resistivity structures, for example, around volcanic regions as potential geothermal energy sources (Aizawa et al. 2011; Hill et al. 2020).

In MT, the primary geomagnetic fields are assumed to be horizontally uniform. If this assumption does not hold because of, for example, localized source currents, MT responses such as the apparent resistivity can be biased (Pirjola 1992; Viljanen et al. 1999; Viljanen 2012; Sato 2020a, 2020b and references therein). For example, Pirjola (1992) derived the biased apparent resistivities between 1 s and 100,000 s resulting from an electrojet with field-aligned currents. Meanwhile, Sato (2020a, 2020b) focused on the shifts in the MT responses stemming from changes in the distances, especially altitudes, between the sites and the source currents. These studies are motivated by the E layer controlling 85–90% of the electrical process during the daytime in the ionosphere, whereas the

F layer controls 50% of this process at night (Maute and Richmond 2017). As a consequence, temporal shifts not caused by changes in the subsurface electrical environment may be detected.

Recently, temporal/seasonal variations (Romano et al. 2014; Vargas and Ritter 2016; Sato et al. 2020) and biases (Murphy and Egbert 2018) in the MT responses, vertical geomagnetic transfer-functions, and inter-station transfer functions resulting from the source field have been reported. Romano et al. (2014) reported a negative correlation between the geomagnetic activity and the apparent resistivities for time periods of 20–100 s. In addition, they showed that the MT responses become unstable when the magnitude of the geomagnetic activity (the Kp or Ap index) is small. In particular, for time-lapse MT soundings, the source-dependent bias within the impedances needs to be considered because we must prevent to misinterpret the shifts as being resulted from temporal changes in the subsurface electrical environment.

On the basis of small site-to-site changes in the MT responses, subsurface resistivity structures can be discussed in detail. Several studies have estimated impedances from short-term measured data, which may be strongly biased by spatially heterogeneous source currents. For example, Ichihara et al. (2019) used MT data acquired over 2–6 days for inverse modeling. Therefore, we need to consider source-dependent biases within the MT responses even if the research target is not a time-varying subsurface environment.

Let us consider the case in which geomagnetic storms do not occur. When the solar activity is quiet or the K index is small, the focus latitude of solar quiet (Sq) currents varies within the range of 20–45° N (Yamazaki and Maute 2017). Conversely, when the solar/geomagnetic activity is disturbed, the focus latitude varies over a small range of approximately 26–38° N. Therefore, MT responses can shift depending on the K index as a result of changes in the distance between the sites and the source currents.

This study first formulates the EM fields at the surface of the Earth arising from source currents that flow within a circle, which is assumed to be a model for the Sq current. Then, I calculate the biased MT responses arising from the Sq currents by varying their centers. Finally, the implications of the obtained results are discussed.

EM fields at the surface of the Earth

We use the SI system and choose a spherical coordinate system, as presented in Figure 1, where the radius of the Earth is set to a, the y-axis corresponds to the North Pole, and the electric current is defined later.

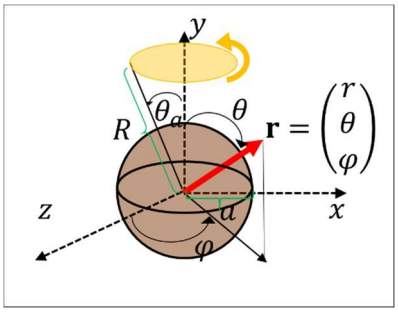

Figure 1. Coordinate system used in this study. $\mathbf{r}$ denotes a position vector.

Because we may ignore the displacement current in MT, Maxwell's equations in the frequency domain are given by

$$\nabla \cdot \mathbf{B} = 0, \tag{1}$$

$$\nabla \cdot \mathbf{E} = 0, \tag{2}$$

$$\nabla \times \mathbf{E} = -i\omega\mathbf{B}, \tag{3}$$

$$\nabla \times \mathbf{B} = \mu_0(\sigma\mathbf{E} + \mathbf{J}^{\mathrm{o}}), \tag{4}$$

where $\mathbf{B}$, $\mathbf{E}$, and $\mathbf{J}^{\mathrm{o}}$ are the magnetic induction, electric field, and external source current, respectively, and i, ω, μ_0, and σ are the imaginary unit, angular frequency, magnetic permeability of free space, and electrical conductivity, respectively. Employing the vector potential $\mathbf{A}$ and the scalar potential Π, the EM fields are represented by

$$\mathbf{B} = \nabla \times \mathbf{A}, \tag{5}$$

$$\mathbf{E} = -i\omega(\mathbf{A} + \nabla\Pi). \tag{6}$$

In MT, we apply a gauge transformation such that

$$\nabla \cdot \mathbf{A} = 0, \tag{7}$$

$$\Pi = 0. \tag{8}$$

As a result, the Helmholtz equation for $\mathbf{A}$ is

$$-\Delta\mathbf{A} + i\omega\sigma\mu_0\mathbf{A} = \mu_0\mathbf{J}^{\mathrm{o}}. \tag{9}$$

Let us consider EM fields at or above the surface of the Earth (i.e., $r \geq a$). Then, σ may be set to zero and the equation for $\mathbf{A}$ is given by

$$-\Delta\mathbf{A} = \mu_0\mathbf{J}^{\mathrm{o}}. \tag{10}$$

For an external source, this study assumes a spherical-sector shell carrying an electric current I (Fig. 1); the current density is

$$\mathbf{J}^{\mathrm{o}} = I\delta(r - R)[H(\theta) - H(\theta - \theta_a)]\begin{pmatrix}0\\0\\1\end{pmatrix}, \tag{11}$$

where δ and H denote the Dirac delta function and the Heaviside step function, respectively. Therefore, the center of the source current corresponds to the North Pole and the current flows counterclockwise at an altitude of $R > a$ and within the colatitude range of $0 \leq \theta \leq \theta_a$. Note that

the Sq current is not located near the North Pole; therefore, the coordinate system needs to be rotated, as described later.

Because the external source $\mathbf{J}^{\mathrm{o}}$ only has a φ-component, we need to solve the Laplace equation in the form

$$\Delta A_\varphi = -\mu_0 I\delta(r-R)[H(\theta)-H(\theta-\theta_a)]. \tag{12}$$

with the Green's function satisfying

$$\Delta G(\boldsymbol{r}-\boldsymbol{r}') = \frac{\delta(r-r')\delta(\theta-\theta')\delta(\varphi-\varphi')}{r^2\sin\theta}. \tag{13}$$

As shown in Arfken et al. (2012) and Sato (2020b), the solution of Eq. (13) is given by

$$G(\boldsymbol{r}-\boldsymbol{r}') = -\frac{1}{4\pi}\sum_{n=0}^{\infty}\sum_{m=-n}^{n}\frac{(n-m)!P_n^m(\cos\theta)P_n^m(\cos\theta')e^{im(\varphi-\varphi')}}{(n+m)!}\left\{\frac{r^n}{(r')^{n+1}}+\frac{c_n}{r'^{n+1}r^{n+1}}\right\}, \tag{14}$$

where c_n is a constant upholding the boundary condition at $r=a$ and P_n^m denotes the associated Legendre polynomials. As a result, A_φ is given by

$$A_\varphi = -\mu_0 I\int_0^{2\pi}d\varphi'\int_0^{\pi}d\theta'\int_a^{\infty}dr'\delta(r'-R)[H(\theta')-H(\theta'-\theta_a)]G(\boldsymbol{r}-\boldsymbol{r}')r'^2\sin\theta', \tag{15a}$$

or

$$A_\varphi = \frac{\mu_0 I}{4\pi}\int_0^{\theta_a}\sum_{n=0}^{\infty}P_n^0(\cos\theta)P_n^0(\cos\theta')\sin\theta'\left\{\frac{r^n}{R^{n-1}}+\frac{c_n}{R^{n-1}r^{n+1}}\right\}d\theta'. \tag{15b}$$

This ensures that $\boldsymbol{\nabla}\cdot\mathbf{A}=0$.

Assuming a structure inside the Earth ($0\le r\le a$) having a homogeneous conductivity σ_1, we only need to solve

$$\Delta A_\varphi - i\omega\sigma\mu_0 A_\varphi = 0. \tag{16}$$

This equation can be solved as shown in Sato (2020b)

$$A_\varphi = \sum_{n=0}^{\infty}\sum_{m=-n}^{n}\left[d_{m,n}j_n(k_1r)+d'_{m,n}y_n(k_1r)\right]e^{\pm im\varphi}P_n^m(\cos\theta), \tag{17}$$

where $k_1=\sqrt{-i\omega\sigma_1\mu_0}$; j_n and y_n denote the spherical Bessel function and spherical Neumann function, respectively; and $d_{m,n}$ and $d'_{m,n}$ are constants that satisfy the boundary condition. Because of its convergence at $r=0$ and $\boldsymbol{\nabla}\cdot\mathbf{A}=0$, Eq. (17) can be rewritten as

$$A_\varphi = \sum_{n=0}^{\infty}d_n j_n(k_1r)P_n^0(\cos\theta). \tag{18}$$

Enforcing the boundary condition, the EM fields at the surface of the Earth (i.e., $r=a$) are given by

$$B_\theta = -\frac{\mu_0 I}{4\pi}\sum_{n=0}^{\infty}(2n+1)P_n^0(\cos\theta)\frac{a^{n-1}}{R^{n-1}}\left[1-\frac{n}{k_1a}\left\{\frac{j_n(k_1a)}{j_{n-1}(ka)}\right\}\right]\int_0^{\theta_a}P_n^0(\cos\theta')\sin\theta'\,d\theta', \tag{19}$$

$$E_\varphi = -i\omega\frac{\mu_0 I}{4\pi}\sum_{n=0}^{\infty}P_n^0(\cos\theta)\frac{a^{n-1}}{R^{n-1}}\left[\frac{(2n+1)j_n(k_1a)}{k_1 j_{n-1}(k_1a)}\right]\int_0^{\theta_a}P_n^0(\cos\theta')\sin\theta'\,d\theta'. \tag{20}$$

Note that j_{-1} may not be defined; however, we can calculate the rate of $\frac{j_n(k_1a)}{j_{n-1}(ka)}$ as

$$\frac{j_n(k_1 a)}{j_{n-1}(k_1 a)} = \frac{J_{n+1/2}(k_1 a)}{J_{n-1/2}(k_1 a)}. \quad (21)$$

The apparent resistivity and phase are defined as

$$\rho = \frac{\mu_0}{\omega}\left|\frac{E_\varphi}{B_\theta}\right|^2, \quad (22)$$

and

$$\phi = \arg\left(\frac{E_\varphi}{B_\theta}\right), \quad (23)$$

respectively. For simplicity, this study expresses lengths (m) and angles (rad) using units of "km" and "degrees," respectively.

Bias within MT responses due to the Sq current

This study assumes two mid-latitude sites (35° N and 40° N). The focus latitude θ_1 of the Sq current is varied in the range of 20–45° N in increments of 1° N. The longitude difference φ_1 between the sites and the source at the moment the electric current flows within the circle is changed from 1° N to 9° N in increments of 1° N. As a result, by rotating the coordinate system so that the center of the source corresponds to the *y*-axis, as shown in Figure 1, we vary only θ in Eqs. (19) and (20). This study defines θ_1 and φ_1 as the focus latitude and the longitude difference, respectively.

The radius of the Earth a and the altitude of the source R are set to 6,400 km and 6,500 km (i.e., the E layer), respectively. The time period is set to 60 s, at which Romano et al. (2014) have shown biased responses from real data. This study uses 0.001 S/m for the conductivity of the Earth (i.e., 1000 ohm-m). As reported in Fig. 49 in Yamazaki and Maute (2017), the electric currents are large, especially within 10–15° from the center (more than approximately 100 kA), and are moderate within 15–20° (approximately 50 kA). Because these ranges and values are not always constant, this study considers only a simple case and varies θ_a from 10° to 20° in increments of 2.5°. When deriving the EM fields at the surface of the Earth (Eqs. (19) and (20)), I use the discrete approximation for the integrals $\int_0^{\theta_a} P_n^0(\cos\theta')\sin\theta'\,d\theta'$ and calculate the summations up to $n = 1000$, with the convergence of each summation being verified. The apparent resistivity and phase are derived following Eqs. (22) and (23), respectively.

The results of the biased MT responses for sites at 35° N and 40° N are presented in Figures 2 and 3, respectively. Both results show that the apparent resistivity and phase deviate greatly from their original values (i.e., 1000 ohm-m and 45°, respectively) if the circumference carrying the currents is near the site, for example, see the results at 40° N obtained from $(\theta_a, \theta_1, \varphi_1) = (10,1,30)$.

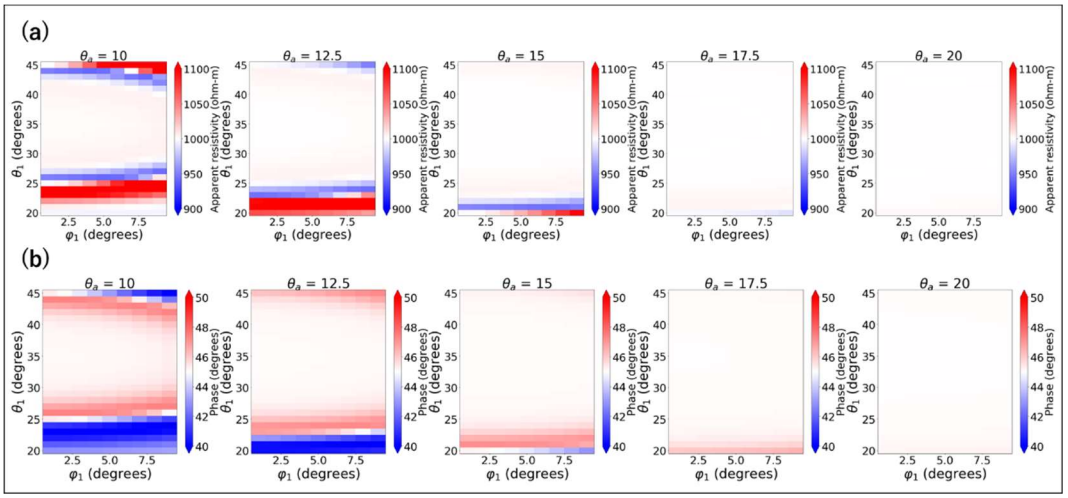

Figure 2. Biased MT responses for a site at 35° N: (a) apparent resistivity and (b) phase. The vertical and horizontal axes denote θ_1 and φ_1 as defined in the text, respectively.

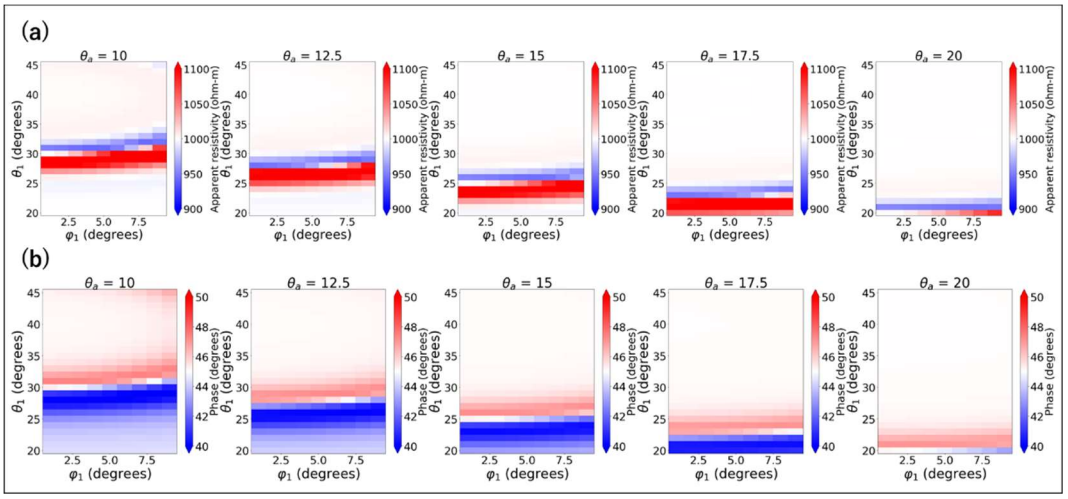

Figure 3. Same as Figure 2 but for a site at 40° N.

Discussion

Here, this study discusses the appropriateness/limitations of the model and the implications of the numerical results (Figs. 2 and 3).

This study employed an electric current flowing within a circle. The equation in the time domain is given by

$$\mathbf{J}^{\mathrm{o}} = I_t \delta(r-R)[H(\theta)-H(\theta-\theta_a)][H(t-t_1)-H(t-t_2)]\begin{pmatrix}0\\0\\1\end{pmatrix}, \tag{24}$$

where $t_1 < t_2$ because MT surveys are possible even when geomagnetic storms do not occur. The current only flows between t_1 and t_2. Note that

$$I_t \int_{t_1}^{t_2} e^{-i\omega t} dt = I, \tag{25}$$

where I is the electric current in Eq. (11). The critical feature of this assumption is that the distance between the source and the sites does not change over time. When estimating the impedances from the EM data, we transformed the time-series data into time-dependent spectra (i.e., into the time–frequency domain) using a short-time Fourier transform (FT), which is a sequence of FTs of tapered time-series data. To derive the spectra at 60 s, we set the FT length to approximately 600 s, within which the temporal shifts in the focus longitude resulting from the rotation of the Earth are approximately 2.5°. Even though the model errors arising from the time-varying focus longitude should be considered, we neglect them here because the numerical simulations (Figs. 2 and 3) are not primarily controlled by φ_1 but rather are primarily controlled by θ_1. As a result, the model for the EM fields at 60 s is considered acceptable. However, if calculating the biased MT responses for a very long period, we would need to consider the fact that the focus longitude shifts significantly over the FT length.

Let us consider the site at 40° N, which was assumed for the MT station in Romano et al. (2014). We set θ_a to 15° because electric currents of approximately 100 kA flow within the modeled range (Yamazaki and Maute 2017). When the geomagnetic activity is disturbed (i.e., when the K or Ap index is large), the focus latitude of the Sq current varies in the range of 26–38° N (Yamazaki and Maute 2017). On the basis of Figure 3, the apparent resistivities and phases appear more downward and upward biased, respectively, than upward and downward biased. When the geomagnetic activity is quiet, the center changes from 20° N to 45° N. The apparent resistivities are not only downward but upward biased, and the phases are not only upward but downward biased. As a result, the apparent resistivities may have a negative correlation with the K index. Even though this interpretation is limited to the case of substituting 15° into θ_a, it is possible to explain the phenomena of unstable MT responses and the negative correlation of the apparent resistivities with the geomagnetic activity reported by Romano et al. (2014).

Supposing that the MT station is located at 35° N, which corresponds to the central area of Japan, when the geomagnetic activity is disturbed ($26° \leq \theta_1 \leq 38°$), the apparent resistivity is not greatly biased by the Sq current. However, quiet geomagnetic activity can yield shifts in the apparent resistivity and phase from the original values if $\theta_a < 17.5°$. Consequently, the MT responses estimated from the data measured when the K index is small may result in incorrect interpretations regarding subsurface resistivity structures.

When estimating impedances from long time-series data (i.e., many spectra), the source-dependent bias may be neglected because the EM fields arising from the Sq current are averaged. Moreover, if geomagnetic storms occur, the MT responses indicate their true values because of the ring currents above the equator (Sato 2020b). However, even if a station is located at mid-latitudes, in

the case of time-lapse MT soundings, especially in a resistive zone, the Sq current effect needs to be considered. For example, we need to check for correlations of the MT responses with the K index and whether the apparent resistivity and phase become unstable when the K index is small. Moreover, even though it might be inconvenient, it is better to only analyze data measured when the geomagnetic activity is disturbed.

Summary

This study focused on biases within the MT responses arising from the Sq current. The numerical simulations indicated that slight variations in the focus latitude cause shifts in the apparent resistivity and phase from their original values. Because the center of the Sq current varies within a range of 20–45° N (small K index) or 26–38° N (large K index), impedances derived from real data may be biased. Even though this study was limited to a specific and simple case, we can explain the phenomena reported in a preceding study, e.g., unstable MT responses due to a small K index and the negative correlation of the apparent resistivities with the geomagnetic activity. As a consequence, even when a station is located at mid-latitudes, we need to consider the biases stemming from the Sq current to interpret time-varying MT responses within resistive areas. These temporal changes need to be treated carefully, for example, by checking the Sq current conditions, the correlation of the impedances with the geomagnetic activity, and whether the MT responses vary with small K indexes. In addition, even though it might be unrealistic, only data measured during large K index periods are suitable for time-lapse MT soundings.

Acknowledgement

The author thanks Mr. Fumihiko Onoue, a Ph.D. candidate at Scuola Normale Superiore di Pisa, for constructive comments.

References

Aizawa K, Kanda W, Ogawa Y, Iguchi M, Yokoo A, Yakiwara H, Sugano T (2011) Temporal changes in electrical resistivity at Sakurajima volcano from continuous magnetotelluric observations. *Journal of Volcanology and Geothermal Research* **199**(1): 165–175.

Arfken GB, Weber HJ, Harris FE (2012) Mathematical methods for physicists: A comprehensive guide. Academic Press, Cambridge.

Evans RL, Hirth G, Baba K, Forsyth D, Chave A, Mackie R (2005) Geophysical evidence from the MELT area for compositional controls on oceanic plates. *Nature* **437**(7056): 249–252.

Hata M, Munekane H, Utada H, Kagiyama T (2020) Three-dimensional electrical resistivity structure beneath a volcanically and seismically active island, Kyushu, Southwest Japan Arc. *Journal of Geophysical Research: Solid Earth* **125**(3): doi.org/10.1029/2019JB017485.

Hill GJ, Bibby HM, Peacock J, Wallin EL, Ogawa Y, Caricchi L, Keys H, Bennie SL, Avram Y (2020) Temporal Magnetotellurics Reveals Mechanics of the 2012 Mount Tongariro, NZ, Eruption. *Geophysical Research Letters* **47**(8): doi.org/10.1029/2019GL086429.

Ichihara H, Mogi T, Satoh H, Yamaya Y (2019) Electrical resistivity modeling around the Hidaka collision zone, northern Japan: regional structural background of the 2018 Hokkaido Eastern Iburi earthquake (Mw 6.6). *Earth, Planets and Space* **71**(1): doi.org/10.1186/s40623-019-1078-7.

Matsuno T, Baba K, Utada H (2020) Probing 1-D electrical anisotropy in the oceanic upper mantle from seafloor magnetotelluric array data. *Geophysical Journal International* **222**(3): 1502–1525.

Maute A, Richmond AD (2017) F-region dynamo simulations at low and mid-latitude. S*pace Science Reviews* **206**: 471–493.

Murphy BS, Egbert GD (2018) Source biases in midlatitude magnetotelluric transfer functions due to Pc3-4 geomagnetic pulsations. *Earth, Planets and Space* **70**(1): doi.org/10.1186/s40623-018-0781-0.

Pirjola R (1992) On magnetotelluric source effects caused by an auroral electrojet system. *Radio Science* **27**(04): 463–468.

Romano G, Balasco M, Lapenna V, Siniscalchi A, Telesca L, Tripaldi S (2014) On the sensitivity of long-term magnetotelluric monitoring in Southern Italy and source-dependent robust single station transfer function variability. *Geophysical Journal International* **197**(3):1425–1441.

Sato S (2020a) Altitude effects of localized source currents on magnetotelluric responses. *Earth, Planets and Space* **72**, doi.org/10.1186/s40623-020-01200-7.

Sato S (2020b) Effects of loop source current on magnetotelluric responses of spherical Earth (in Japanese). *BUTSURI-TANSA (Geophysical Explorations)* **73**: 168–176.

Sato S, Goto T, Koike K (2020a) Spatial gradients of geomagnetic temporal variations causing the instability of inter-station transfer functions. *Earth, Planets and Space* **72**, doi.org/10.1186/s40623-020-01231-0.

Vargas JA, Ritter O (2016) Source effects in mid-latitude geomagnetic transfer functions. *Geophysical Journal International* **204**(1):606–630.

Viljanen A (2012) Description of the magnetospheric/ionospheric sources. In: Chave AD, Jones AG (ed) The Magnetotelluric Method. Cambridge University Press, Cambridge.

Viljanen A, Pirjola R, Amm O (1999) Magnetotelluric source effect due to 3D ionospheric current systems using the complex image method for 1D conductivity structures. *Earth, planets and space* **51**(9): 933–945.

Yamazaki Y, Maute A (2017) Sq and EEJ–A review on the daily variation of the geomagnetic field caused by ionospheric dynamo currents. *Space Science Reviews* **206**: 299–405.